Achieving Both Giant d_{33} and High T_C in Patassium-Sodium Niobate Ternary System

Xiaojing Cheng,[†] Jiagang Wu,*,[†] Xiaojie Lou,[‡] Xiangjian Wang,[‡] Xiaopeng Wang,[†] Dingquan Xiao,[†] and Jianguo Zhu[†]

[†]Department of Materials Science, Sichuan University, Chengdu 610064, P. R. China

[‡]Multi-disciplinary Materials Research Center, Frontier Institute of Science and Technology, and State Key Laboratory for Mechanical Behavior of Materials, Xi'an Jiaotong University, Xi'an 710049, P. R. China

ABSTRACT: Both giant d_{33} and high T_C have been obtained in a lead-free piezoelectric ternary system $(0.995 - x)K_{0.48}Na_{0.52}NbO_3$-$0.005BiScO_3$-$xBi_{0.5}(Na_{0.7}K_{0.2}Li_{0.1})_{0.5}ZrO_3$. Thanks to the rhombohedral-tetragonal phase coexistence and the enhanced dielectric and ferroelectric properties, the ceramic with a composition of $x = 0.04$ shows a giant d_{33} of ~366 pC/N together with T_C of ~335 °C, thereby paving the way for achieving both high d_{33} and high T_C in KNN-based materials. In addition, such a ceramic has a good thermal stability of d_{33} (e.g., $d_{33} > 319$ pC/N, $T \leq 300$ °C) and an enhanced stability of ferroelectric properties against temperature. The domain-wall energy barrier of ~0.15 eV is derived from the temperature dependence of the back-switching polarization.

KEYWORDS: lead-free piezoelectrics, ternary system, R-T phase boundary, piezoelectricity, high Curie temperature
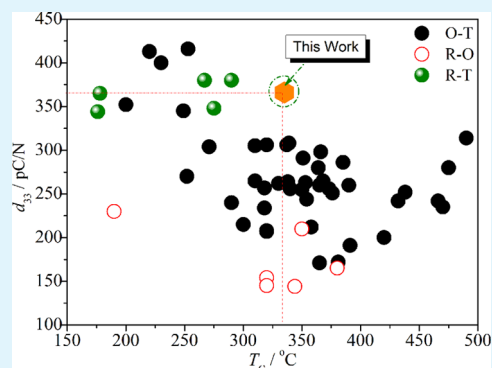
INTRODUCTION

In the last decades, there has been an increasing amount of efforts, exemplified by many experimental and theoretical studied in the literature, in searching for new high-performance lead-free piezoelectrics.[1−6] From those works published previously, it is clear that it is extremely difficult to achieve both high piezoelectric constant (d_{33}) and high Curie temperature (T_C) in a single piezoelectric ceramic. Currently, $(K,Na)NO_3$ (KNN), a lead-free piezoelectric with promising properties, is facing the same dilemma [See Figure 1].[1,4,6−13] However, to replace the lead-based piezoelectric ceramics, such as Lead Zirconate Titanate (PZT), it is an indispensible task to

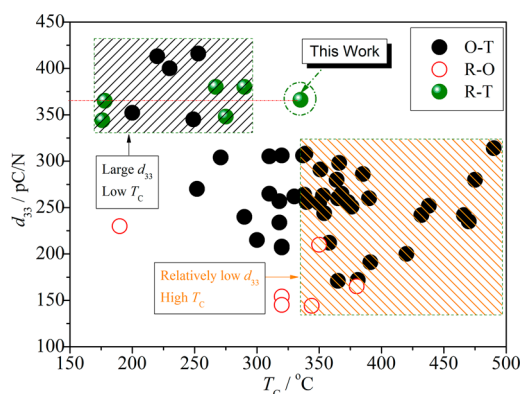**Figure 1.** Comparison of d_{33} and T_C of KNN-based ceramics derived from the work published previously and those in this work.

achieve a good comprehensive performance of d_{33} and T_C in KNN. Recently, a considerable amount of effort has been made to achieve this objective. The main attempts include new preparation techniques,[1,14] the construction of phase boundary,[1,4,6−9,15−24] and so forth. Unfortunately, it is difficult to obtain a giant d_{33} and a high T_C simultaneously in the KNN-based system.[1,4,6−9,13,14,16−23] For example, it was reported that a giant d_{33} of 400−413 pC/N could be obtained in Li^{+}, Ta[5+], and Sb[5+] -modfied KNN ceramics by using the orthorhombic-tetragonal (O-T) phase boundary. However, a low T_C of ≤220 °C was unavoidably observed.[7,25] More recently, the construction of a new rhombohedral-tetragonal phase boundary has been used to enhance KNN's piezoelectricity.[8,9,23] Although a high d_{33} of 344−425 pC/N was obtained, their T_C is very low (e.g., ≤200 °C). Therefore, the contradiction between high d_{33} and high T_C remains as an unsolved problem for KNN-based materials, hindering their practical high-temperature piezoelectric applications.

In the present work, we developed a new material system, $(0.995-x)K_{0.48}Na_{0.52}NbO_3$-$0.005BiScO_3$-$xBi_{0.5}(Na_{0.7}K_{0.2}Li_{0.1})_{0.5}ZrO_3$, abbreviated as $(0.995-x)$KNN-0.005BS-xBNKLZ, for solving the contradictory relationship between high d_{33} and high T_C. In this material system, adding $BiScO_3$ can concurrently increase T_{R-O} and decrease T_{O-T} of KNN ceramics,[26−28] as the BNKLZ[12] and Sb[5+29] do. Finally, it

Figure 2. XRD results of the ceramics in the 2θ range of (a) 20−60°, (b) 21−23°, and (c) 43−47°.

was observed that both a giant d_{33} of ∼366 pC/N and a high T_C of ∼335 °C could be obtained by tailoring the composition of such a material system. It was found that the comprehensive performance of d_{33} and T_C achieved in this work is superior to the reported results in other KNN-based materials, as shown in Figure 1. The underlying mechanisms are discussed with the aim of understanding the enhanced piezoelectric properties of the KNN-based ceramics.

■ EXPERIMENTAL SECTION

The material system of (0.995 − x)KNN-0.005BS-xBNKLZ (x = 0−0.07) was prepared using the conventional solid-state method. Na_2CO_3 (99.8%), K_2CO_3 (99%), Bi_2O_3 (99.999%), Nb_2O_5 (99.5%), Li_2CO_3 (98%), Sc_2O_3 (99.999%), and ZrO_2 (99%) were used as raw materials. All disk samples were sintered at 1080−1150 °C for 3 h in air after the PVA binder was burnt out. All samples have been polarized in a silicone oil bath at 30 °C under a *dc* field of 3.0−4.0 kV/mm for 20 min. Other detailed preparation process and measurement methods have been described elsewhere.[23]

■ RESULTS AND DISCUSSION

Figure 2a shows the XRD results of the (0.995 − x)KNN-0.005BS-xBNKLZ (x = 0−0.07) ceramics in the 2θ range of 20−60°. We can see from Figure 2a that a perovskite structure could be observed for all the ceramics. To identify the phase structure of this material system, detailed XRD analysis was conducted in the 2θ range of 21−23 and 43−47°, as displayed in panels b and c in Figure 2. The composition dependence of phase structure of the ceramics is clearly observed. It was found that the XRD patterns in 2θ = 21−23 and 43−47° give a better illustration on the phase evolution induced by increasing the BNKLZ doping level. From panels b and c in Figure 2, one sees that the ceramics with $x \leq 0.02$ show an orthorhombic phase at room temperature, similar to a pure KNN.[4,21,22,30] As the BNKLZ content increases, the orthorhombic and tetragonal phases coexist in the ceramics with 0.02 < $x \leq 0.035$. It is worth noting that the ceramics with 0.045 $\leq x \leq$ 0.07 show a remarkably broadened permittivity band in comparison with those with other composition, as shown in Figure 3a. It was previously reported that the fine-grained ceramics, such as $BaTiO_3$,[31] $PbTiO_3$,[32] $Pb_{0.98}(Zr_{0.52}Ti_{0.48})_{0.92}Nb_{0.004}O_3$,[33] and $Pb_{0.98}(Zr_{0.52}Ti_{0.48})_{0.92}O_3$,[33] show a significant broadened permittivity peak. As a result, the decrease in grain sizes may account for the broadening in the permittivity peak of the ceramics with 0.045 $\leq x \leq$ 0.07 (see Figures 3a and 4d).
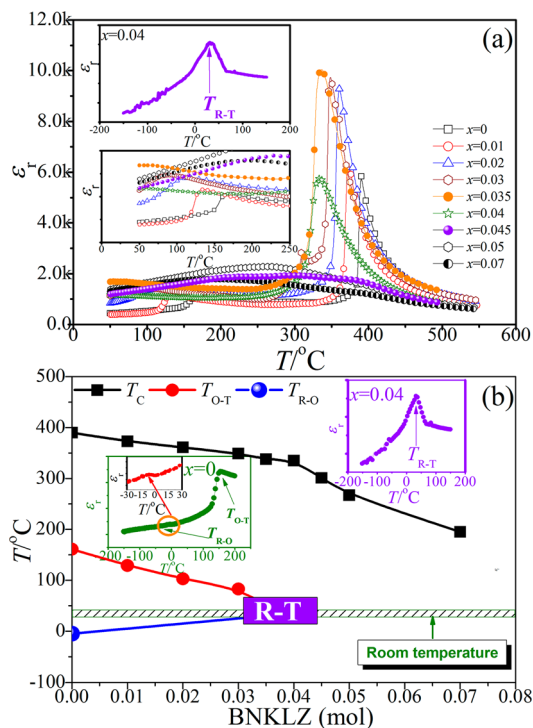

Figure 3. (a) Profile of ε_r versus temperatures; the inset shows the profiles of ε_r as a function of temperature at −150 to 200 °C, and 50−250 °C for the ceramic with x = 0.04. (b) Phase diagram of the ceramics as a function of the BNKLZ content.

Finally, the rhombohedral-tetragonal phase coexistence is observed in the ceramics with the composition of 0.035 < x < 0.045, which could be further confirmed by the temperature-dependent dielectric results in −150−200 °C (see Figure 3a, b).

Figure 3a shows the dielectric constant (ε_r) of the ceramics against temperature measured at f = 100 kHz for different compositions or x. The ceramics with $x \leq$ 0.03 demonstrate two phase transformations above room temperature, corresponding to that from an orthorhombic phase to a tetragonal phase ($T_{O\text{-}T}$) and that from a tetragonal phase to a cubic phase (T_C),[1,3,4,10] as shown in the inset of Figure 3. Adding more BNKLZ can shift both $T_{O\text{-}T}$ and T_C of KNN to lower temperatures.[12] As the BNKLZ concentration further increases ($x \geq$ 0.04), the $T_{O\text{-}T}$ peak at room temperature finally disappears. A clear dielectric peak is observed in the ceramic with x = 0.04 by measuring the temperature-dependent
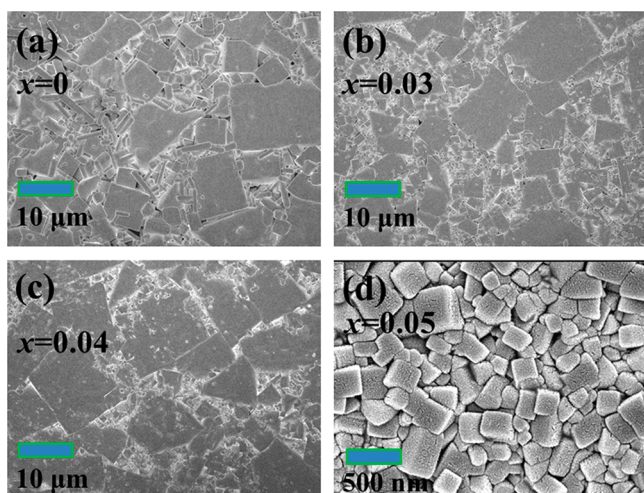
Figure 4. SEM micrographs of the surface morphologies of the ceramics with different BNKLZ levels: (a) $x = 0$, (b) $x = 0.03$, (c) $x = 0.04$, and (d) $x = 0.05$.

dielectric behavior in $-150-200$ °C (see the inset of Figure 3a). In this work, the BNKLZ level could tune both T_{O-T} and T_{R-O} of KNN,[12] as BiScO$_3$ does.[26] In other words, both T_{O-T} and T_{R-O} are shifted close to room temperature with increasing BNKLZ concentration. Finally, the R and T phases were found to coexist in the ceramic with $x = 0.04$ (see Figure 3b). In spite of the significant broadening of the ε_r vs T peak in the ceramics with $0.045 \leq x \leq 0.07$ (see Figure 3a), it was found that the ferroelectric-paraelectric transition temperature could still be defined as the point at which ε_r reaches the maximum.[31] In the literature, phase diagram has been widely used to describe the phase evolution of ferroelectric materials.[2,12,20,23,24,34] In this work, the phase diagram of the $(0.995 - x)$KNN-0.005BS-xBNKLZ ceramics was established, according to the temperature-dependent ε_r in Figure 3a. One can see from Figure 3b that the plateau in the profile of T_C vs the BNKLZ level is evident for $x \leq 0.04$, and then the T_C curve drops linearly for $x > 0.04$, demonstrating that a high T_C is well-maintained at low BNKLZ doping concentrations. In addition, the T_{O-T} curve gradually decreases and the T_{R-O} curve increases as the BNKLZ content increases, and finally both T_{O-T} and T_{R-O} "converge" at room temperature. As a result, the R-T phase coexistence could be achieved in the ceramic with $x = 0.04$ around room temperature.

To investigate the effect of the BNKLZ content on ceramic morphologies, we carried out FE-SEM studies on the surface morphologies of the ceramics, as shown in Figures 4a–d. We can observe from Figure 4a–d that their surface morphologies can be tailored by changing the BNKLZ doping level. In addition, it is worth noting that the ceramics with $x \leq 0.04$ show a bimodal grain size distribution, where small grains are located at the gaps of large ones, resulting in a dense microstructure. To characterize the element distribution of the ceramic with $x = 0.04$, we conducted element mapping on the ceramic surface by using EDX analysis, as displayed in Figure 5. These results imply that all the elements in the ceramic are homogeneously distributed.

Figure 6a shows the $P-E$ hysteresis loops of the ceramics, which were measured using a triangle waveform of 10 Hz at room temperature. A squared hysteresis loop could be observed in the ceramics with $x < 0.045$, while a slim $P-E$ loop was recorded in the fine-grained ceramics with $x \geq 0.045$.[33] To further show the variation in ferroelectric properties with the BNKLZ doping level, P_r and E_c, obtained from the $P-E$ loops, were shown in Figure 6b. One can see that P_r shows a plateau for $x \leq 0.04$, and then drops as the BNKLZ concentration increases $(x \geq 0.045)$ because of the appearance of fine grain.[12,33] In contract, E_C first increases and then drops as the BNKLZ level increases, with the maximum value peaked at $x = 0.035$. Therefore, it can be concluded that adding BNKLZ (<0.045) could enhance the ferroelectricity of the ceramics.

Figure 7a–d shows the temperature-dependent ferroelectric properties of the ceramic with $x = 0.04$, which demonstrates the best properties among all the ceramics studied in this work. Figure 7(a) displays the $P-E$ hysteresis loops of the ceramic with $x = 0.04$ at the measurement temperature range of $30-180$ °C. Clearly, one sees that there is only a slight variation in the $P-E$ loops as the temperature rises from 30 to 180 °C, demonstrating a good temperature stability of its ferroelectric properties. Panels b and c in Figure 7 plot the spontaneous polarization (P_s), the remanent polarization (P_r), and the coercive field (E_C) as a function of temperatures, which were all obtained from the $P-E$ loops shown in Figure 7a. P_s, P_r, and E_C all drop as measurement temperature increases. It is well-known that the loss of alkali metal during sintering gives rise to the formation of K$^+$ and Na$^+$ vacancies as well as $V_O^{\cdot\cdot}$ in KNN,[35−37] and the $V_O^{\cdot\cdot}$−Nb^{4+} dipole is believed to be strongly associated with the thermally activated process in KNN-based materials.[38,39] In addition, it was reported that more intensive thermal fluctuation at higher temperatures can promote domain switching and lower the activation energy for oxygen vacancy diffusion, both of which result in a significant decrease in E_C as temperature increases.[3,40,41] Furthermore, the reduction in lattice distortion with increasing temperature can also facilitate the reorientation of domains, giving rise to a lower E_C as well as
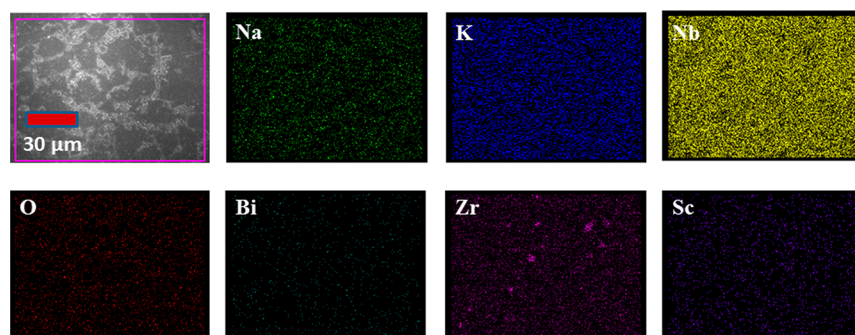

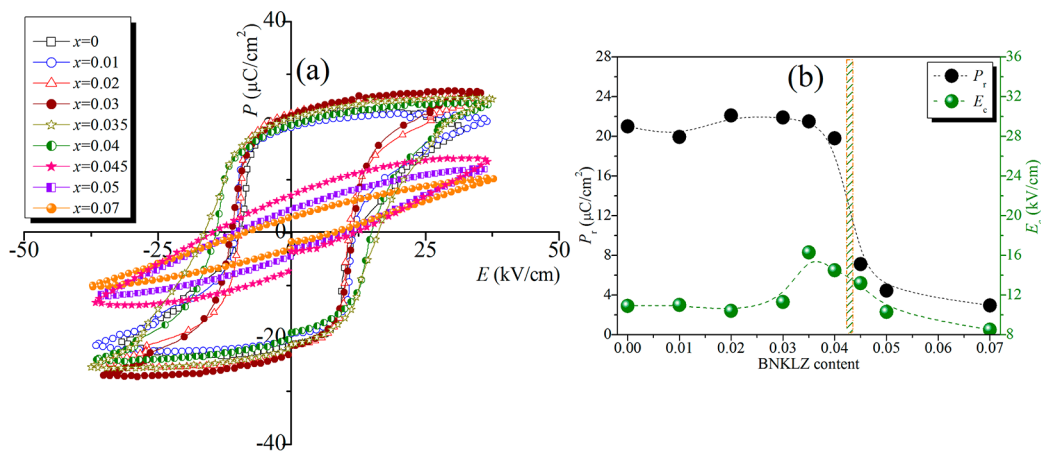**Figure 5.** Element mapping of the ceramics with $x = 0.04$.

752

dx.doi.org/10.1021/am404793e | *ACS Appl. Mater. Interfaces* 2014, 6, 750−756

Figure 6. (a) P−E loops for different BNKLZ levels, and (b) P_r and E_c versus the BNKLZ level obtained from a.
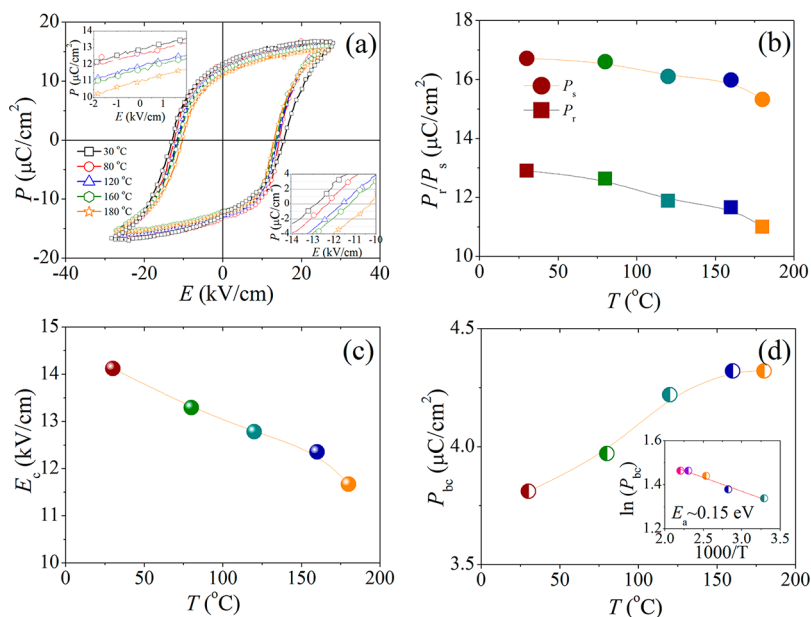

Figure 7. (a) P−E hysteresis loops of the ceramics with $x = 0.04$, measured at various temperatures; (b) the profiles of P_s, and P_r; (c) that of E_c; (d) and that of the back-switching polarization (P_{bc}) vs measurement temperature obtained from a; the inset in d shows the curve of $\ln(P_{bc})$ vs $1000/T$.
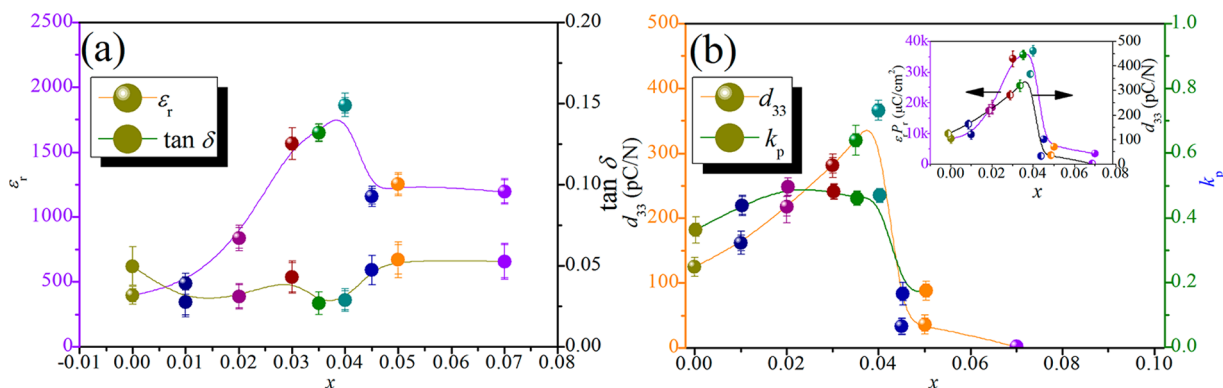

Figure 8. (a) ε_r and $\tan \delta$, and (b) d_{33} and k_p of the ceramics as a function of the BNKLZ concentration, and the inset in (b) shows the profile of $\varepsilon_r P_r$ and d_{33} of the ceramics against the BNKLZ content.

a slimmer P−E loop.[42] From panels b and c in Figure 7, we see that when temperature increases from 30 to 180 °C, P_r shifts slightly from 12.7 to 11.0 μC/cm², P_s descends a little from 16.6 to 15.3 μC/cm², and E_C decreases from 13.29 to 11.67

kV/cm. Such a slight change in P_s and P_r with temperature demonstrates excellent thermal stability of its ferroelectric properties. The effect of "polarization back switching" is defined as the switching process in which highly polarized domains
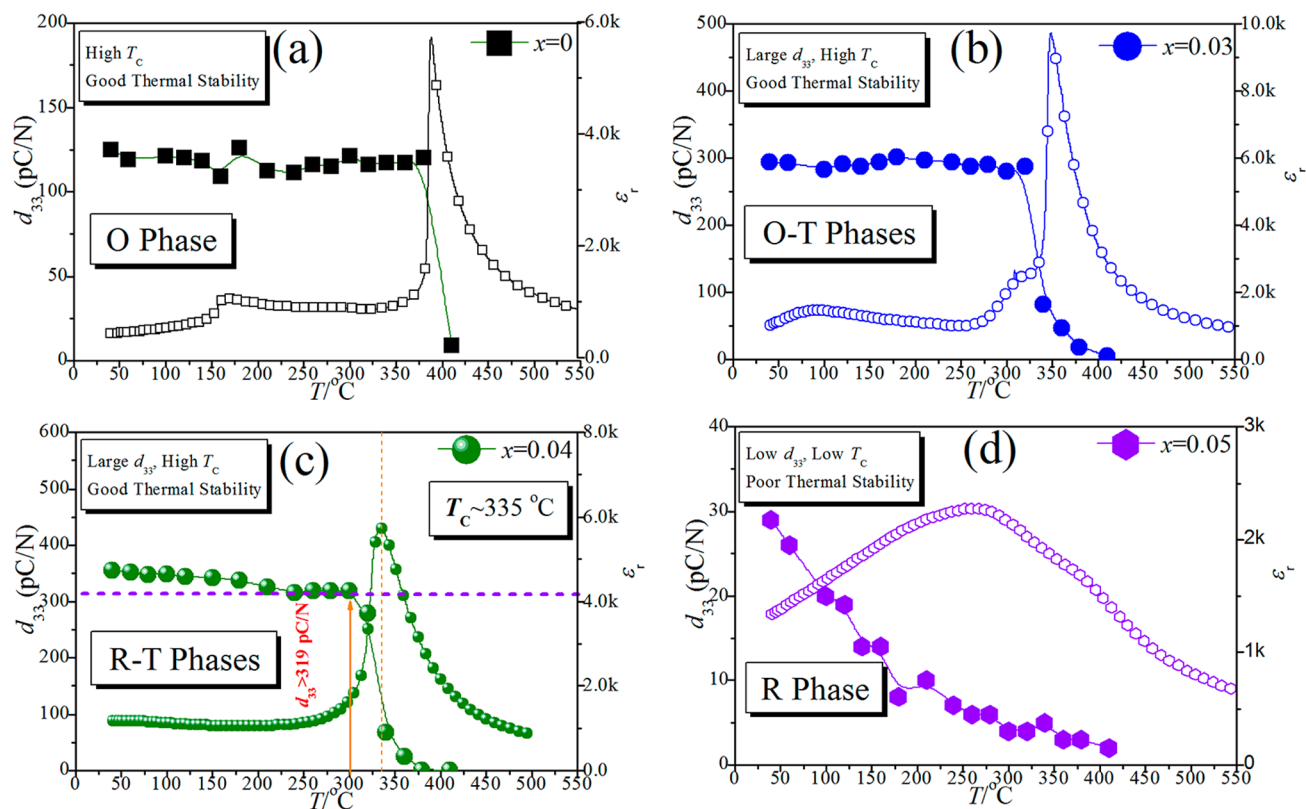
Figure 9. Thermal stability of d_{33} in a temperature range of 30−550 °C for different BNKLZ contents: (a) $x = 0$, (b) $x = 0.03$, (c) $x = 0.04$, and (d) $x = 0.05$.

tend to be depolarized to some extent and form configurations of lower energy, driven by the residue depolarization field upon the removal of the external field.[43] The back-switched polarization (P_{bc}) can be written as $P_{bc} = P_s − P_r$.[44] From Figure 7d, one sees that P_{bc} increases from 3.97 to 4.32 $\mu C/cm^2$ as temperature increases from 30 to 180 °C . From the thermal activation point of view, P_{bc} could be written as[44]

$$P_{bc} = P_0 \exp(−E_a/k_B T) \tag{1}$$

where E_a and T represent the activation energy for domain wall movement and the absolute temperature, respectively; and k_B and P_0 are the Boltzmann constant and a fitting constant, respectively. A plot of $\ln(P_{bc})$ vs $1000/T$ is displayed in the inset of Figure 7d. E_a of 0.15 eV could be obtained for the ceramic with $x = 0.04$, which could be tentatively attributed to the movement of singly ionized oxygen vacancies, coming from the loss of alkali metal during sintering[35−37] and a thermally activated process for the $V_O^{\cdot\cdot}−Nb^{4+}$ dipole .[38,39]

Figure 8a plots ε_r and tan δ of the ceramics as a function of x, measured at 100 kHz and room temperature. We can see from Figure 8a that ε_r is strongly dependent on the BNKLZ concentration x. ε_r increases almost linearly when x is lower than 0.04, and then drops dramatically as the BNKLZ level further increases. The largest ε_r can be observed in the ceramic with its composition lying in the phase boundary region.[45,46] The reason for the decrease in ε_r of the ceramics with $0.045 \leq x \leq 0.07$ is attributed to refined grain sizes[31−33] (see Figure 4d). On the other hand, all the ceramics studied in this work show a low tan δ, and the lowest tan δ was observed in the ceramics with $x = 0.035−0.04$. Figure 8b shows k_p and d_{33} of the ceramics as a function of the BNKLZ concentration x. Remarkably, it was found that enhanced piezoelectric proper-

ties could be achieved in the ceramic with $x = 0.04$, with its d_{33} ≈ 366 pC/N and k_p ≈ 0.47. Therefore, a comprehensive performance with both high d_{33} and high T_C was obtained in this work, which is superior to the reported results on other KNN-based materials, as shown in Figure.1. Thus, we conclude that the R-T phase coexistence plays a crucial role in enhancing the piezoelectric properties of the $(0.995 − x)$KNN-0.005BS-xBNKLZ systems.[8,9,12] The reasons for the enhanced electrical properties of piezoelectric materials by constructing the R-T phase boundary are listed below:[15,41,47−53] the coexistence of R and T phases in lead-based materials is believed to be the origin of their large piezoelectricity due to the existence of two thermodynamically equivalent phases during the poling process, and the resultant appearance of highly oriented domains.[15,41,47,48] In addition, the flattening of the free-energy profile may also contribute to the enhanced properties in such a phase transition region, as confirmed by Ab initio and phenomenological calculations.[49−53] The easy paths for polarization change were determined by the anisotropy of the free energy profile.[52] As a result, the material system studied in this work shows an enhanced piezoelectric behavior near its MPB region, which is similar to that of PZT, as shown in Figure 8. Moreover, it was also believed that the larger d_{33} obtained in this work comes partly from the higher $\varepsilon_r P_r$ (e.g., d_{33} ≈ $\alpha \varepsilon_r P_r$).[3,54] To show this in a clearer manner, we show the curves of d_{33} and $\varepsilon_r P_r$ vs the BNKLZ content in the inset of Figure 8b. We can see that the profiles of d_{33} and $\varepsilon_r P_r$ show similar trends as the BNKLZ doping level increases. Both d_{33} and $\varepsilon_r P_r$ become maximized in the ceramic with $x = 0.04$, implying that $\varepsilon_r P_r$ indeed shows strong correlation with d_{33}.

Higher d_{33} and better thermal stability always contradict with each other in KNN-based ceramics due to the existence of a

polymorphic phase transition near room temperature,[1,3,7,10,19] which seriously affects their practical applications. In the current work, the thermal stability of d_{33} is investigated, as shown in Figure 9. We can see from Figure 9 that the thermal stability of d_{33} is strongly dependent on the phase structure of the ceramics. The ceramic containing an O phase shows a thermally stable d_{33} due to the involvement of the O phase,[55,56] as shown in panels a and b in Figure 9. However, the d_{33} thermal stability of the ceramics containing R and T phases deteriorates slightly, and an almost linear drop is observed for the fine-grained ceramics containing merely an R phase (Figure 9d). As a result, the change in the d_{33} thermal stability studied in this work could be attributed to the involvement of different phase structures. Figure 9c plots the thermal stability of the ceramics with $x = 0.04$. One sees that d_{33} descends gradually from 366 to ca. 319 pC/N as the temperature rises from room temperature up to 300 °C. Then, d_{33} decreases dramatically as the temperature is close T_C. As a result, it was found that the ceramic with $x = 0.04$ demonstrates a good thermal stability of d_{33} in 25−300 °C. Furthermore, the R-T phase boundary investigated in this work is similar to those of lead-containing piezoelectric material.[57−59] The peak in the ε_r vs T profile corresponding to the R-T phase boundary has also been recorded in lead-containing materials, in which a good temperature stability of piezoelectric properties is observed.[57−59] As a result, the good thermal stability of d_{33} discovered in this work may be due to the formation of an R-T phase boundary with a morphotropic character.

CONCLUSION

We have realized the objective of achieving both a giant d_{33} and a high T_c in the KNN -based system, along with good temperature stability of d_{33}. The phase coexistence of rhombohedral and tetragonal phases was found to lie in the ceramic with the composition of $x = 0.04$, in which an enhanced piezoelectric properties has been observed. In addition, a low BiScO$_3$ content was found to give rise to a higher T_C in the KNN-based material. We report that the ceramic with $x = 0.04$ shows the optimum electrical behavior of $d_{33} \approx 366$ pC/N, $k_p \approx 0.47$, $\varepsilon_r \approx 1863$, tan $\delta \approx 2.86\%$, and $T_C \approx 335$ °C, together with a good thermal stability ($d_{33} > 319$ pC/N) for $T \leq 300$ °C. The existence of an R-T phase boundary and the associated enhanced dielectric and ferroelectric properties are thought to be responsible for the improvement in d_{33}. We believe that the system is a promising candidate for high-temperature lead-free piezoelectric applications in the future.

AUTHOR INFORMATION

Corresponding Author
*E-mail: msewujg@scu.edu.cn and wujiagang0208@163.com.

Notes
The authors declare no competing financial interest.

ACKNOWLEDGMENTS

REFERENCES

(1) Saito, Y.; Takao, H.; Tani, T.; Nonoyama, T.; Takatori, K.; Homma, T.; Nagaya, T.; Nakamura, M. *Nature* **2004**, *432*, 84−87.
(2) Liu, W.; Ren, X. *Phys. Rev. Lett.* **2009**, *103*, 257602.
(3) Zhang, S.; Xia, R.; Shrout, T. R.; Zang, G.; Wang, J. *J. Appl. Phys.* **2006**, *100*, 104108.
(4) Guo, Y.; Kakimoto, K.; Ohsato, H. *Appl. Phys. Lett.* **2004**, *85*, 4121−4123.
(5) Sasaki, A.; Chiba, T.; Mamiya, Y.; Otsuki, E. *Jpn. J. Appl. Phys.* **1999**, *38*, 5564−5567.
(6) Hollenstein, E.; Davis, M.; Damjanovic, D.; Setter, N. *Appl. Phys. Lett.* **2005**, *87*, 182905.
(7) Gao, Y.; Zhang, J.; Qing, Y.; Tan, Y.; Zhang, Z.; Hao, X. *J. Am. Ceram. Soc.* **2011**, *94* (9), 2968−2973.
(8) Zuo, R.; Fu, J. *J. Am. Ceram. Soc.* **2011**, *94*, 1467−1470.
(9) Liang, W. F.; Wu, W. J.; Xiao, D. Q.; Zhu, J. G.; Wu, J. G. *J. Mater. Sci.* **2011**, *46*, 6871−6876.
(10) Rödel, J.; Jo, W.; Seifert, K.; Anton, E. M.; Granzow, T.; Damjanovic, D. *J. Am. Ceram. Soc.* **2009**, *89*, 1153−1177.
(11) Damjanovic, D.; Klein, N.; Li, J.; Porokhonskyy, V. *Funct. Mater. Lett.* **2010**, *3*, 5−13.
(12) Cheng, X.; Wu, J.; Wang, X.; Zhang, B.; Zhu, J.; Xiao, D.; Wang, X.; Lou, X. *Appl. Phys. Lett.* **2013**, *103*, 052906.
(13) Zang, G. Z.; Wang, J. F.; Chen, H. C.; Su, W. B.; Wang, C. M.; Qi, P.; Ming, B. Q.; Du, J.; Zheng, L. M.; Zhang, S.; Shrout, T. R. *Appl. Phys. Lett.* **2006**, *88*, 212908.
(14) Zhang, B. P.; Li, J. F.; Wang, K.; Zhang, H. *J. Am. Ceram. Soc.* **2006**, *89*, 1605−1609.
(15) Damjanovic, D. *Appl. Phys. Lett.* **2010**, *97*, 062906.
(16) Ge, W.; Ren, Y.; Zhang, J.; Devreug, C. P.; Li, J.; Viehland, D. *J. Appl. Phys.* **2012**, *111*, 103503.
(17) Akdoğan, E. K.; Kerman, K.; Abazari, M.; Safari, A. *Appl. Phys. Lett.* **2008**, *92*, 112908.
(18) Klein, N.; Hollenstein, E.; Damjanovic, D.; Trodahl, H. J.; Setter, N.; Kuball, M. *J. Appl. Phys.* **2007**, *102*, 014112.
(19) Hollenstein, E.; Damjanovic, D.; Setter, N. *J. Eur. Ceram. Soc.* **2007**, *27*, 4093−4098.
(20) Skidmore, T. A.; Comyn, T. P.; Bell, A. J.; Zhu, F.; Milne, S. J. *IEEE Trans. Ultrason. Ferroelectr. Freq. Control* **2011**, *58* (9), 1819−1825.
(21) Wu, J. G.; Xiao, D. Q.; Wang, Y. Y.; Zhu, J. G.; Wu, L.; Jiang, Y. H. *Appl. Phys. Lett.* **2007**, *91* (25), 252907.
(22) Wu, J.; Wang, Y.; Xiao, D.; Zhu, J.; Pu, Z. *Appl. Phys. Lett.* **2007**, *91*, 132914.
(23) Zhang, B. Y.; Wu, J. G.; Cheng, X. J.; Wang, X. P.; Xiao, D.; Zhu, J.; Wang, X.; X. Lou, X. *ACS Appl. Mater. Interface* **2013**, *5* (16), 7718−7725.
(24) Cheng, X. J.; Wu, J. G.; Wang, X. P.; Zhang, B. Y.; Lou, X. J.; Wang, X. J.; Xiao, D. Q.; Zhu, J. G. *ACS Appl. Mater. Interface* **2013**, *5* (21), 10409−10417.
(25) Zuo, R.; Fu, J.; Lv, D. *J. Am. Ceram. Soc.* **2009**, *92* (1), 283−285.
(26) Zuo, R. Z.; Ye, C.; Fang, X. S. *Jpn. J. Appl. Phys.* **2007**, *46* (10A), 6733−6736.
(27) Zhu, F.; Ward, M. B.; Comyn, T. P.; Bell, A. J.; Milne, S. J. *IEEE Trans. Ultrason. Ferroelectr. Freq. Control* **2011**, *58* (9), 1811−1818.
(28) Skidmore, T. A.; Comyn, T. P.; Milne, S. J. *J. Am. Ceram. Soc.* **2010**, *93* (3), 624−626.
(29) Zuo, R. Z.; Fu, J.; Lv, D. Y. *J. Am. Ceram. Soc.* **2010**, *93* (9), 2783−2787.
(30) Egerton, L.; Dillon, D. M. *J. Am. Ceram. Soc.* **1959**, *42*, 438−442.
(31) Zhao, Z.; Buscaglia, V.; Viviani, M.; Buscaglia, M. T.; Mitoseriu, L.; Testino, A.; Nygren, M.; Johnsson, M.; Nanni, P. *Phys. Rev.* **2004**, *B70*, 024107.
(32) Chattopadhyay, S.; Ayyub, P.; Palkar, V. R.; Multani, M. *Phys. Rev.* **1995**, *B52*, 13177.

(33) Randall, C. A.; NamchulKim; Kucera, J. P.; Cao, W. W.; Shrout, T. R. *J. Am. Ceram. Soc.* **1998**, *81* (3), 677−688.

(34) Noheda, B.; Cox, D. E.; Shirane, G.; Gao, J.; Ye, Z. G. *Phys. Rev.* **2002**, *B66*, 054104.

(35) Matsubara, M.; Yamaguchi, T.; Kikuta, K.; Hirano, S. *Jpn. J. Appl. Phys.* **2005**, *44* (Part 1), 258−263.

(36) Tashiro, S.; Nagamatsu, H.; Nagata, K. *Jpn. J. Appl. Phys.* **2002**, *41* (Part1), 7113−7118.

(37) Matthias, B. T.; Remeika, J. P. *Phys. Rev.* **1951**, *82*, 727−729.

(38) Kizaki, Y.; Noguchi, Y.; Miyayama, M. *Appl. Phys. Lett.* **2006**, *89*, 142910.

(39) Miao, J.; Xu, X. G.; Jiang, Y.; Cao, L. X.; Zhao, B. R. *Appl. Phys. Lett.* **2009**, *95*, 132905.

(40) Damjanovic, D. *Rep. Prog. Phys.* **1998**, *61*, 1267−1324.

(41) Yimnirun, R.; Ngamjarurojana, A.; Wongmaneerung, R.; Wongsaenmai, S.; Ananta, S.; Laosiritaworn, Y. *Appl. Phys.* **2007**, *A 89*, 737−741.

(42) Du, G.; Liang, R.; Wang, L.; Li, K.; Zhang, W.; Wang, G.; Dong, X. *Appl. Phys. Lett.* **2013**, *102*, 142903.

(43) Picinin, A.; Lente, M. H.; Eiras, J. A.; Rino, J. P. *Phys. Rev.* **2004**, *B69*, 064117.

(44) Ma, B.; Hu, Z.; Liu, S.; Narayanan, M.; Balachandran, U. *Appl. Phys. Lett.* **2013**, *102*, 072901.

(45) Jaffe, B.; Cook, W. R.; Jaffe, H. *Piezoelectric Ceramics*; Academic Press: London, 1971.

(46) Eitel, R. E.; Randall, C. A.; Shrout, T. R.; Park, S. E. *Jpn. J. Appl. Phys.* **2002**, *41*, 2099−2104.

(47) Jaffe, B.; Roth, R. S.; Marzullo, S. *J. Appl. Phys.* **1954**, *25*, 809−810.

(48) Smolenskii, G. A. *Ferroeletrics and Related Materials*; Taylor, G. W., Ed.; Gordon and Breach; New York, 1984.

(49) Fu, H.; Cohen, R. E. *Nature* **2000**, *403*, 281−283.

(50) Wu, Z. G.; Cohen, R. E. *Phys. Rev. Lett.* **2005**, *95*, 037601.

(51) Budimir, M.; Damjanovic, D.; Setter, N. *Phys. Rev.* **2006**, *B73*, 174106.

(52) Damjanovic, D. *J. Am. Ceram. Soc.* **2005**, *88*, 2663−2676.

(53) Ishibashi, Y.; Iwata, M. *Jpn. J. Appl. Phys.* **1999**, *38* (Part1), 800−804.

(54) Shrout, T. R.; Zhang, S. *J. Electroceram.* **2007**, *19*, 111−124.

(55) Gao, Y.; Zhang, J. L.; Zong, X. J.; Wang, C. L.; Li, J. C. *J. Appl. Phys.* **2010**, *107*, 074101.

(56) Lin, D.; Li, Z.; Zhang, S.; Xu, Z.; Yao, X. *Solid State Commun.* **2009**, *149*, 1646−1649.

(57) Li, F.; Zhang, S.; Xu, Z.; Wei, X.; Luo, J.; Shrout, T. R. *J. Appl. Phys.* **2010**, *108*, 034106.

(58) Zhang, S.; Lee, S. M.; Kim, D. H.; Lee, H. Y.; Shrout, T. R. *Appl. Phys. Lett.* **2007**, *90*, 232911.

(59) Zhang, S.; Luo, J.; Hackenberger, W.; Shrout, T. R. *J. Appl. Phys.* **2008**, *104*, 064106.